Evaluation of ocean surface waves along the coastal area of the Sea of Okhotsk during winter

S. Iwasaki[1] and J. Otsuka[1]

[1]Civil Engineering Research Institute for Cold Region, 1–3–1–34 Toyohira, Sapporo 062–8602, Japan.

Corresponding author: Shinsuke Iwasaki (iwasaki-s@ceri.go.jp)

Key Points:

- Six wave-ice parameterization models are evaluated using the buoy observation in the Sea of Okhotsk.
- The empirical model in which the attenuation rate depends on the frequency is found to be the most stable.
- Simulation with sea ice significantly improved the bias of wave fields in the coastal area compared to the simulation without sea ice.

Abstract

Ocean surface waves tend to be attenuated on interaction with sea ice. In this study, six sea ice models were implemented in the third-generation wave model WAVEWATCH III® (WW3) to estimate wave attenuation by sea ice. The models were evaluated using buoy observations in the coastal area of the Sea of Okhotsk (SO). Additionally, the impact of sea ice on wave fields was demonstrated by model experiments with and without the utilization of sea ice. As a result, one of the empirical models strongly agrees with the buoy observation. The simulation with sea ice drastically improved the bias of wave fields in coastal areas compared to simulation without sea ice. Moreover, the impact of sea ice reached more than 1 m (3 s) for the monthly significant wave height (period). These results suggest that the effect of sea ice on wave calculation is essential in the SO.

Plain Language Summary

It is postulated that sea ice is decreasing in the Sea of Okhotsk (SO) due to the effects of global warming. It is a matter of great concern that the ocean surface wave of the SO will increase, owing to the decrease in sea ice. This study is a first-cut analysis of the evaluation of wave calculation and the effect of sea ice on waves in the SO.

1 Introduction

The Sea of Okhotsk (SO) is a marginal ice zone (defined as the region of an ice cover that is affected by waves and swell penetrating into the ice from the open ocean) and is the southernmost sea with a sizeable seasonal ice cover in the Northern Hemisphere. Accurate calculation of ocean surface waves in the SO is important for ensuring safe shipping routes and identifying hazardous areas. In addition to its social importance, ocean waves in sea ice are a part of the interaction between sea ice, the ocean, and the atmosphere, and is essential to understand climate change. In winter, sea ice rapidly extends southeastward from November to March, and thereafter it reduces (Figure 1a–g). Sea ice suppresses the wave-wind interaction by reducing fetch. It also modifies the wave dispersion relation, and the wave energy is attenuated through a conservative scattering and non-conservative dissipation phenomenon (Squire, 2020). Although the sea ice extent in the SO has large interannual variability, its maximum value has been reported to decrease at a rate of 3.9 %/decade on the Japan Meteorological Agency (JMA) website (https://www.data.jma.go.jp/gmd/kaiyou/english/seaice_okhotsk/series_okhotsk_e.html). Therefore, it is of concern that a decrease in sea ice in the SO will result in an increase in ocean surface waves in the future.

WAVEWATCH III® (WW3; WAVEWATCH® Development Group, 2019), one of the most widely used third-generation spectral wave models based on the radiative transfer equation for global and regional wave forecasts, has implemented several parameterizations for wave-ice interaction. In deep water, when currents are absent, the evaluation of wind-generated ocean waves is governed by:

$$\frac{\partial N}{\partial t} + \nabla \cdot C_{\mathrm{g}} N = \frac{S}{\sigma}, \tag{1}$$

where N=E/σ is the wave action density spectrum, which is a function of wave number or radian frequency(k or σ), direction(θ), space(x, y), and time(t), E is the wave energy spectral density, and $\boldsymbol{C}_{\mathbf{g}}$ is the group velocity. For ice-covered region, the sum of the source term on the right-hand side of Eq. (1) is defined as follows:

$$S = (1 - C_{\mathrm{i}})(S_{\mathrm{in}} + S_{\mathrm{ds}}) + S_{\mathrm{nl}} + C_{\mathrm{i}} S_{\mathrm{ice}}, \tag{2}$$

where S_{in} is the input term by wind, S_{ds} is the dissipation term induced by wave breaking, S_{nl} is the nonlinear interaction term among spectral components, S_{ice} is the wave-ice interaction term, and C_{i} is the ice concentration. Both wind input and dissipation terms (S_{in} and S_{ds}) are scaled by the open water fraction($1 - C_{\mathrm{i}}$), whereas S_{ice} is scaled by the ice concentration. The effects of ice on ocean waves can be presented as a complex wavenumber $k = k_{\mathrm{r}} + ik_{\mathrm{i}}$, with the real part k_{r} representing the physical wave number related to the wave length and propagation speeds, producing effects analogous to shoaling and refraction by bathymetry, and the imaginary part k_{i} representing the exponential attenuation coefficient $k_{\mathrm{i}} = k_{\mathrm{i}}(x, y, t, \sigma)$ which depends on the location, time, and radian frequency. k_{i} is introduced in the WW3 model as:

$$\frac{S_{\mathrm{ice}}}{E} = -C_{\mathrm{g}}\alpha = -2C_{\mathrm{g}}k_{\mathrm{i}}, \tag{3}$$

Here, α is the exponential attenuation rate for wave energy, which is twice that of the amplitude ($\alpha = 2k_{\mathrm{i}}$). The above equation (Eq. 3) is used to calculate the dissipation by ice in WW3, denoted as IC1–5 (except for IC0).

Recently, studies have compared and evaluated some wave–ice parameterization models of the WW3 using field observations in the Arctic Sea, in regions such as the Barents Sea (Liu et al., 2020), Chukchi Sea (Nose et al., 2020), and Beaufort Sea (Cheng et al., 2020). Although, sea ice can be expected to have a significant impact on the wave fields, no studies have evaluated the effect of sea ice on the wave field in the SO. This study evaluates the wave fields derived from six wave–ice parameterization models (IC0–5 in WW3) using the Nationwide Ocean Wave Information Network for Ports and Harbours (NOWPHAS) buoy observations (see Text S2 and Figure 1h). Moreover, the impact of sea ice on wave fields using model simulations with and without sea ice were also clarified.

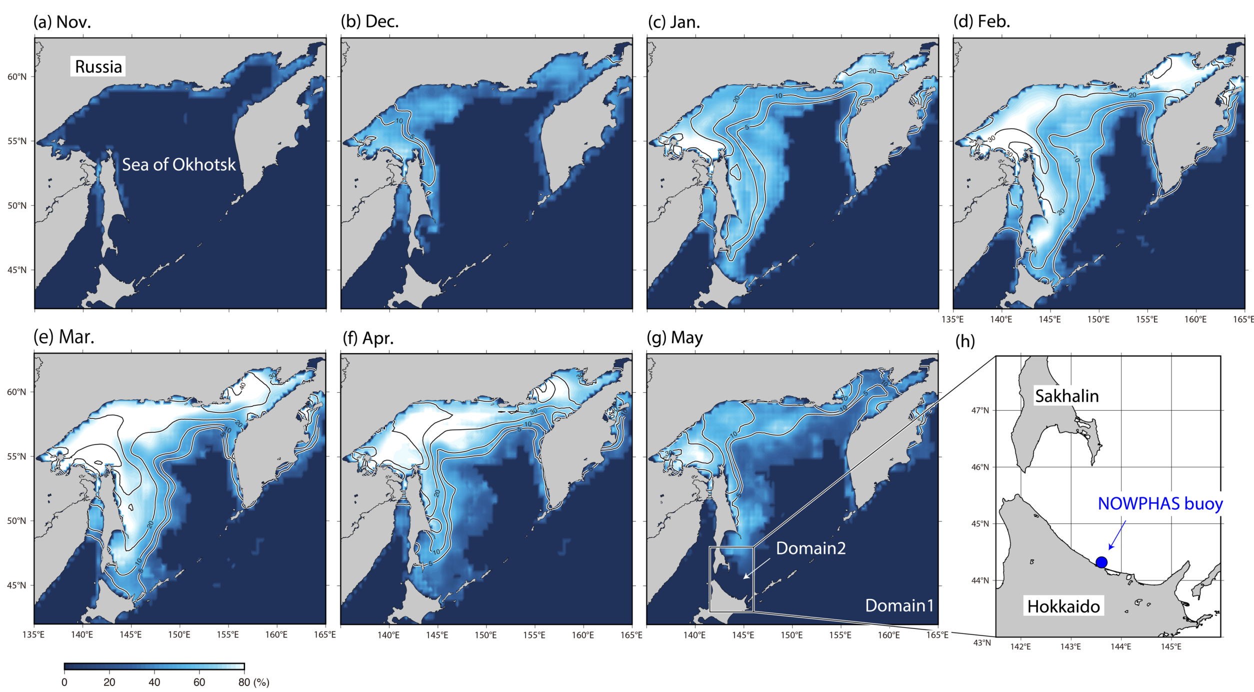

Figure 1. Monthly ice concentration (color) and ice thickness (contour) from November to May during 2008–2010 incorporating two model domains. (**a**–**g**) represents the ice concentration and ice thickness derived from NOAA OI SST V2 and CFSR, respectively. CFSR ice thickness (cm) were smoothed with a two-dimensional boxcar filter with a width of 50 km. (**h**) The blue dot shows the NOWPHAS buoy location.

2 Model design

Two model domains were created using a nesting process, for a horizontal resolution of 0.25° (domain 1) and 0.08° (domain 2) (Figure 1g). The outer domain (domain 1) covers the entire SO (42°–63°N, 135°–165°E). The inner domain (domain 2) was used for the validation of wave fields in the coastal area (43°–48°N, 141.5°–146°E). The directional resolution was 10°, and the frequency space was 0.035–1.1 Hz, which was logarithmically discretized into 30 increments. GEBCO2020 was used to provide the bottom topography and coastlines.

The simulation of domain 1 was driven incorporating 6-hourly surface wind data from the Japanese 55-year Reanalysis (JRA55) (Kobayashi et al., 2015) from the JMA. This product is approximately 55 km in latitude and longitude. In addition, the wind data for domain 2 were obtained from JRA55's dynamic regional downscaling product (DSJRA55) (Kayaba et al., 2016) developed by JMA, in which the product has a spatial resolution of 5 km and a temporal resolution of 1 h. Daily ice concentration was obtained from NOAA Optimum Interpolation (OI) sea surface temperature (SST) version 2 high-resolution dataset with a 0.25° × 0.25° spatial grid (Reynolds et al. 2007). Ice thickness was incorporated from the Climate Forecast System Reanalysis (CFSR) produced by NCEP (Saha et al., 2010). The thickness product has a spatial resolution of 0.25° at the equator, extending to a global 0.5° beyond the tropics, with a temporal resolution of 6 h. The wind, ice concentration, and thickness data were linearly interpolated to the same spatial grid in the wave simulation of both the domains.

In this study, six models for S_{ice}, IC0, IC1, IC2, IC3, IC4, and IC5 were used. Only IC4 is different from the other models and provides seven empirical formulas denoted as IC4M1–M7 (see Text S1). In addition, in order to investigate the impact of sea ice on the wave field, a simulation without incorporating ice concentration was conducted. Hereinafter, the model results without ice concentration are denoted as "Non-ICE". Although IC4M5 and IC4M6 both provide a step function in the frequency space, IC4M6 has more steps than IC4M5. Therefore, IC4M5 was excluded from validation in this study. A simple diffusive scattering model (denoted as IS1 in WW3) was used for these simulations. Another scattering model (denoted as IS2) was implemented in WW3. However, the difference between the scattering models (i.e., IS1 and IS2) was small compared to the difference between the dissipation models (IC0–IC5) (not shown). For terms S_{in} and S_{ds}, we used both ST4 (Ardhuin et al., 2010; Rascle & Ardhuin, 2013) and ST6 (Rogers et al., 2012; Zieger et al., 2015; Liu et al., 2019). All simulations were performed over a three-year period from 2008 to 2010. The significant wave height (H_s) and mean wave period (T_{m01}) were both saved every hour during the computation period. To obtain the modeled value at the buoy position, we linearly interpolated the fields to the buoy position using the surrounding four grid values from domain 2. The significant wave period (T_s) of the model simulation was derived using the following equation: T_s = 1.2T_{m01} (Goda, 2010).

3 Results

3.1 Validation with buoy

To visualize the standard deviation (STD), root mean square error (RMSE), and correlation coefficient between the model simulations and NOWPHAS buoy, Figure 2 displays Taylor diagrams between the two fields (Taylor, 2001). In addition, Table 1 lists the statistical values between the model simulation and buoy observations for H_s and T_s. Here, IC4M2 is the simulation result of IC4M6H2 as this result demonstrated relatively better accuracy (see Table S3). In addition, the results of IC4M6 are not presented here as IC4M6 can be almost reproduced by the binomial fitting of IC4M2 (see Tables S3 and S4). In the present study, we utilized values only when the ice concentration in the coastal area (44°–46°N, 142.5°–145.5°E) around the buoy was 10% or more (except in Figures 3–5). The number of validation data points were 3277. For H_s, all model simulations indicate a correlation coefficient greater than 0.75, a normalized STD between 0.99 and 1.4, and a normalized RMSE and RMSE of less than 0.8 and 0.5 m, respectively (Figure 2a and Table 1). The bias for all H_s simulation was within ± 0.3 m except for IC0 (Table 1). The RMSE and the correlation coefficients of IC1 and IC4M2 were 0.4 m and 0.83, respectively, which were better than those of other simulations (Table 1), although a normalized STD of both simulations slightly overestimates as presented in Figure 2a. In contrast, the bias, normalized RMSE, and RMSE of IC0 were 0.47, 0.82, and 0.51 m, respectively, which were poorly estimated as compared with other simulations Figure. 2a and Table 1). Overall, for T_s, all simulations provided corresponding correlation coefficients of less than 0.73, which was relatively worse than those of H_s (Figure. 2 and Table 1). In addition, the differences in the statistical values between simulations were large compared to those of H_s (Figure 2 and Table 1). A normalized STD for IC0, IC1, and IC4M4 was less than 0.8, which tends to be underestimated (Figure 2b). Moreover, IC4M1 and IC4M7 were poorly simulated, as the correlation coefficients in both simulations were less than 0.5 (Table 1). In contrast, IC3, IC4M2, and IC5 were simulated with least number of errors and indicated a normalized STD from 1 to 1.1, and a normalized RMSE (RMSE) of less than approximately 0.9 (2 s) (Figure 2b and Table 1). In particular, the bias for IC4M2 was 0.02 s, smaller than those of IC3 and IC5 (Table 1).

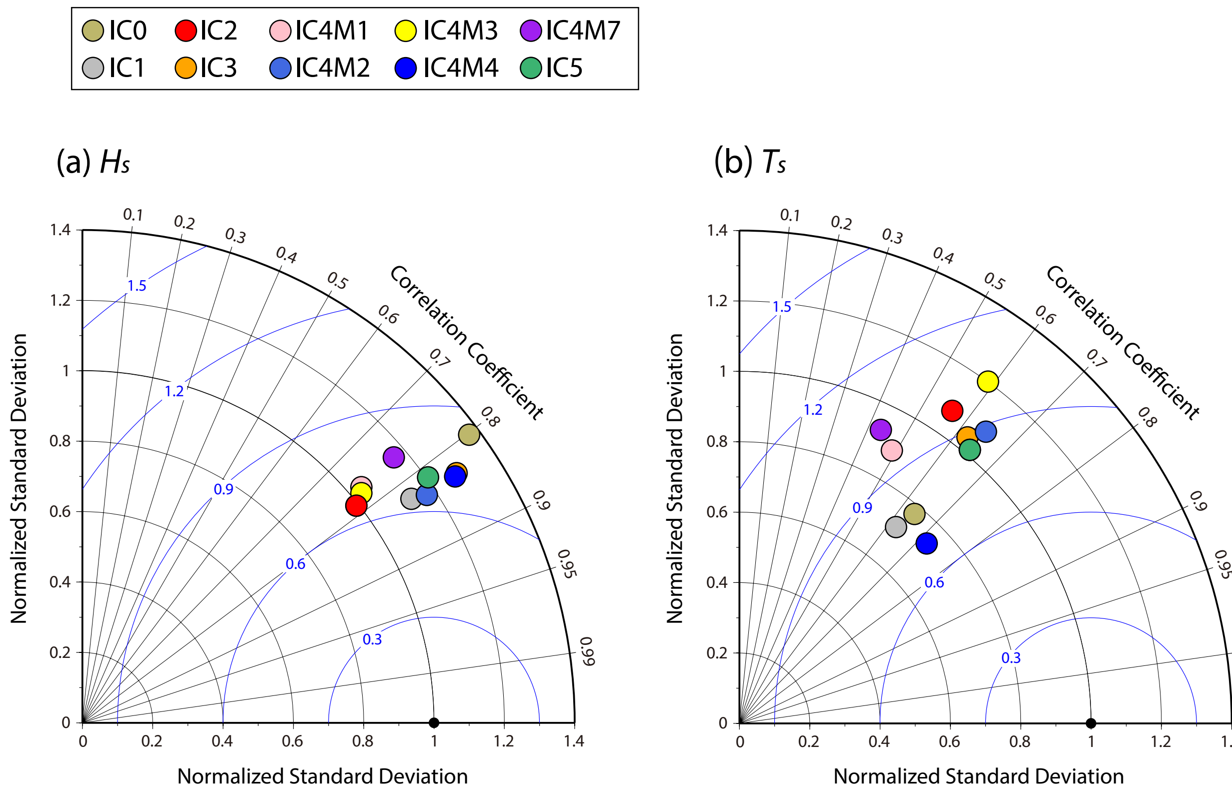

Figure 2. Taylor diagram summarizing the statistical comparison between the NOWPHAS buoy observation and the model simulations with ST6: (**a**) H_s and (**b**) T_s. The source terms of S_{ice} are represented by the different colored-markers in legend in the upper region of the panel. The black circle at the bottom indicates the buoy observation. The blue colored contour with an interval of 0.3 denotes the RMSE between the simulations and observations. The RMSE and standard deviations have been normalized by the observed standard deviation. The correlation coefficients between both the fields are shown by the azimuthal position of the simulation field.

Table 1. *Statistical values of H_s and T_s between model simulations and buoy observation.*

	IC0	IC1	IC2	IC3	IC4M1	IC4M2	IC4M3	IC4M4	IC4M7	IC5
H_s										
Bias (m)	0.47	0.10	0.01	0.27	-0.07	0.08	-0.06	0.29	0.10	0.17
RMSE (m)	0.51	0.40	0.41	0.44	0.44	0.40	0.43	0.44	0.47	0.43
Corr.	0.80	0.83	0.78	0.83	0.76	0.83	0.77	0.83	0.76	0.82
T_s										
Bias (s)	0.67	-0.82	-0.07	0.66	-1.48	0.02	-0.92	0.00	-0.79	-0.20
RMSE (s)	1.74	1.75	2.17	1.97	2.14	1.96	2.26	1.54	2.29	1.89
Corr.	0.64	0.62	0.56	0.62	0.49	0.65	0.59	0.72	0.43	0.64

Moreover, we validated the model simulations as a function of ice concentration (Figure 3). All H_s simulations were overestimated at low ice concentrations (C_{i} < 20 %) (Figure 3a). At high ice concentrations (C_{i} > 20%), the tendency differed depending on the simulation (Figure 3a). IC0, IC3, and IC4M4 were overestimated, while IC4M1 and IC4M3 tended to underestimate (Figure 3a). IC1 and IC4M2 were relatively close to the buoy observations and were simulated with high accuracy, consistent with the comparison shown in Figure 2a and Table 1. For T_s, the difference G between the simulations became remarkable as the ice concentration increased (Figure 3b). IC4M2 and IC4M4 were in good agreement with the observations (Figure 3b). IC1, IC4M1, IC4M3, and IC4M7 were underestimated, especially for IC4M1 and IC4M7 at C_{i} > 40% (Figure 3b). On the other hand, the T_s of IC0 and IC3 were overestimated, regardless of ice concentration (Figure 3b).

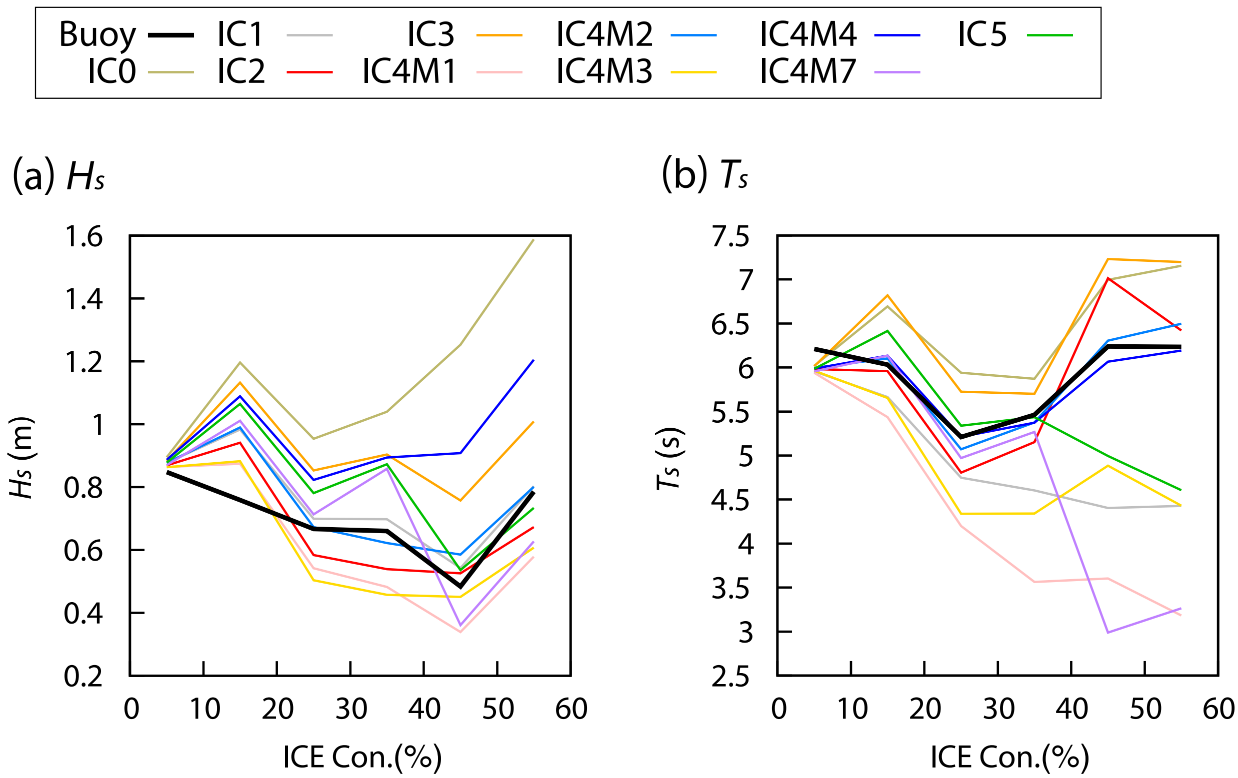

Figure 3. (**a**) H_s and (**b**) T_s averaged from the ST6 model simulations and NOWPHAS buoy as a function of ice concentration in 10% bins. The source terms of S_{ice} represented by the different colored lines are interpreted in the legend of the figure. The horizontal axis denotes the ice concentration in the coastal area around the buoy (44°–46°N, 142.5°–145.5°E).

3.2 Sea ice impact for wave field

To evaluate the impact of sea ice on ocean waves in the SO, we compared the non-ICE simulations and IC4M2, which are relatively accurate. Figure 4 shows the monthly H_s and T_s for the simulation and observation at the buoy position. In general, large H_s and T_s were observed in the coastal areas of Hokkaido during winter (Figure 4). Interestingly, IC4M2 simulations remarkably improved the overestimation of H_s and T_s of Non-ICE simulations from January to April, when sea ice existed (i.e., ice concentration is not 0%) Figure 4).

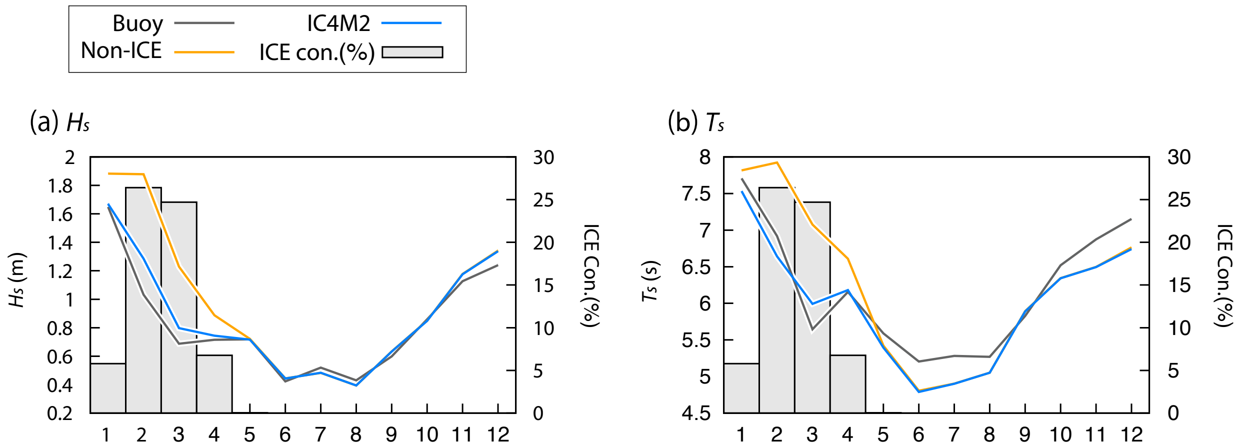

Figure 4. Temporal variations of monthly (**a**) H_s and (**b**) T_s derived from the simulation and the buoy observation. The line colors and bars are defined in the legend in the upper left corner. As shown in the legend in the upper left corner, different colored lines are used for the buoy observation (gray), IC4M2 simulation (light blue), and Non-ICE simulation (yellow). Both simulations are modeled results with ST6. Values are averaged each month from 2008 to 2010. The light gray bars represent the ice concentration in the coastal area around buoy (44°–46°N, 142.5°–145.5°E).

Figure 5 shows the spatial distribution of H_s and T_s from IC4M2 in February, and the differences between IC4M2 and non-ICE. As expected, the wave fields were strongly dependent on the sea ice field, and H_s (T_s) became smaller (larger) as the ice concentration increased (Figures. 5a, b). The H_s (T_s) difference between IC4M2 and non-ICE is greater (less) than 1 m (3 s) at high ice concentrations (C_{i} >70%) (Figure 5).

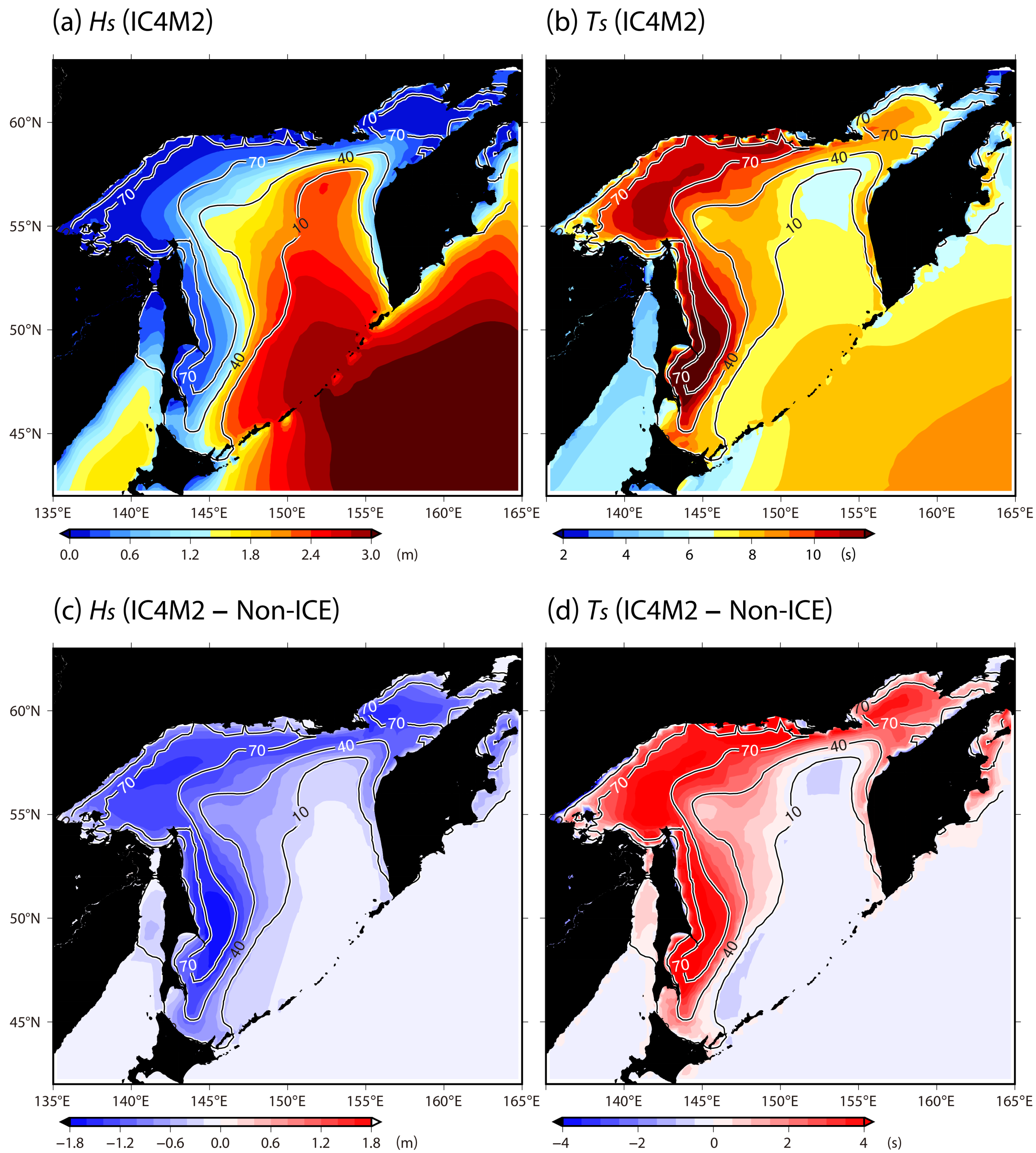

Figure 5. Averaged field (color) of (**a**) H_s and (**b**) T_s computed by IC4M2 in February during 2008–2010; its difference (color) between IC4M2 and Non-ICE simulations; (**c**) H_s; (**d**) T_s. Spatial

smoothing using a box filter of horizontal scale 50 km was performed for the ice concentration (contour) (%). In this figure, we used the model results from domain 1.

4 Summary and Discussion

In this study, we evaluated six wave–ice parameterization models (IC0–IC5) using buoy observations. We also clarified the impact of sea ice on wave fields over the SO. As a result, IC4M2 appears to agree mostly with buoy observation. We also clarified the impact of sea ice on wave fields over the SO. In the coastal area, the simulation with sea ice drastically improved the bias of wave fields (H_s and T_s) compared to that without the use of sea ice. In addition, the difference between the simulation with and without sea ice is more than 1 m (3 s) for the monthly mean H_s (T_s). These results suggest that the effect of sea ice on wave calculation is essential not only in the Arctic and Antarctic Oceans but also in the SO.

Various coefficients have been proposed for the binomial fitting of IC4M2 based on different observational data (Text S1 and Table S1). In the eight simulation results of IC4M2, the bias of IC4M6H1, WA3 UK, and WA3 NIWA were greater than 0.15 m (0.45 s) in H_s (T_s), which was larger than the other simulations (Table S2). In fact, the attenuation rates of IC4M6H1, WA3 UK, and WA3 NIWA were lower than those of the other (Figure S1).

Our validation demonstrated that the accuracy of IC4M1, IC4M3, and IC4M7 was poor (especially in T_s), and the attenuation rate was significantly different from that of IC4M2 (Figure S2). This is probably because the sea ice conditions based on these parameterizations are different from those of the SO. The sea ice thickness is less than 10 cm in the coastal area of Hokkaido (Figure 1). In addition, the floe size of sea ice is from 1.19 m to 5 m in the coastal area of Hokkaido (Kioka et al., 2020). In contrast, IC4M1 uses field data with sea ice floe sizes ranging from 20 m to 30 m. In addition, IC4M3 is based on the ice thickness between 0.5 m and 3m, which is much thicker than the ice conditions in this study. Moreover, IC4M7 is based on observations of only the pancake ice region, although both pancake and frazil ice may exist in the SO.

The accuracy of theoretical models IC2, IC3, and IC5 is not very poor, despite the use of the default theoretical ice parameters, which remains questionable in the SO. Recently, Liu et al. (2020) quantified the kinematic viscosity (ν) used in IC2, the ν and the effective shear modulus

(G) in IC3, based on field observations in the Barents Sea. If the optimum theoretical ice parameters for the SO can be quantified, improvements in these theoretical models can be expected.

ST4 is a source term of S_{in} and (S_{ds}), which is often used in addition to ST6. As described in Section 2, we also evaluated six dissipation models (IC0–IC5) with ST4 (Figure S3, S4, and S5). Overall, there were no significant differences in the wave fields between ST4 and ST6 in the buoy location (Figure S3, Tables 1, and S5). However, the normalized STD for H_s with ST4 was remarkably reduced (approximately 0.16) compared with that of ST6 (Figure S3, Tables 1, and S5). When examined as a function of ice concentration, H_s and T_s with ST4 were slightly smaller than those with ST6, but the tendency in both simulations remained the same (Figure S4).

Recently, Nose et al. (2020) revealed that the uncertainty between ice concentration products is greater than the uncertainty between theoretical models (IC2, IC3, and IC5). Thus, it should be noted that our results depend not only on the parameterization for source terms such as S_{in}, S_{ds}, and S_{ice}, but also on the ice concentration used as forcing. In addition, the theoretical models IC2, IC3, and IC5 also depend on the ice thickness. Moreover, differences in wind data may also be one of the causes of uncertainty in wave fields.

Acknowledgments

We are grateful to data providers including the Ports and Harbours Bureau, Ministry of Land, Infrastructure, Transport, and Tourism (MLIT) for NOWPHAS buoy (https://www.mlit.go.jp/kowan/nowphas/index_eng.html), NOAA for OISST version 2 (https://psl.noaa.gov/data/gridded/data.noaa.oisst.v2.highres.html), NCEP for CFSR (https://rda.ucar.edu/datasets/ds093.1), and JMA for JRA55 (https://rda.ucar.edu/datasets/ds628.0) and DSJRA55 (https://jra.kishou.go.jp/DSJRA-55/index_en.html).

References

Ardhuin, F., Rogers, E., Babanin, A.V., Filipot, J.F., Magne, R., Roland, A., Van Der Westhuysen, A., Queffeulou, P., Lefevre, J.M., Aouf, L. & Collard, F. (2010). Semiempirical dissipation source functions for ocean waves. Part I: Definition, calibration, and validation. *Journal of Physical Oceanography*, *40(9)*, 1917–1941.

Cheng, S., Stopa, J., Ardhuin, F., & Shen, H.H. (2020). Spectral attenuation of ocean waves in pack ice and its application in calibrating viscoelastic wave-in-ice models. *Crysphere*, 14, 2053–2069. https://doi.org/10.5194/tc-14-2053-2020

Goda, Y. (2010). Random Seas and Design of Marin Structures. *World Scientific.* https://doi.org/10.1142/7425

Kayaba, N., Yamada, T., Hayashi, S., Onogi, K., Kobayashi, S., Yoshimoto, K., Kamiguchi, K. & Yamashita, K. (2016). Dynamical regional downscaling using the JRA-55 reanalysis (DSJRA-55). *SOLA*, 12, 1–5.

Kioka, S., Ishida, M., Hasegawa, T., Takeuchi, T., & Saeki, H. (2020). A study of sea ice floe distribution on Okhotsk Sea coast of Hokkaido. *Proceedings of civil engineering in the ocean*. 76, I_905– I_910. https://doi.org/10.2208/jscejoe.76.2_I_905

Kobayashi, S., Ota, Y., Harada, Y., Ebita, A., Moriya, M., Onoda, H., Onogi, K., Kamahori, H., Kobayashi, C., Endo, H. & Miyaoka, K. (2015). The JRA-55 reanalysis: General specifications and basic characteristics. *Journal of the Meteorological Society of Japan. Ser. II*, *93*(1),5–48.

Liu, D., Tsarau, A., Guan, C., & Shen, H. H. (2020). Comparison of ice and wind-wave in WAVEWATCH III ○R in the Barents sea, *Cold Regions and Science Technology.* 172, https://doi.org/10.1016/j.coldregions.2020.103008

Liu, Q., Rogers, W. E., Babanin, A. V., Young, I. R., Romero, L., Zieger, S., Qiao, F., & Guan, C. (2019). Observation-Based Source Terms in the Third-Generation Wave Model WAVEWATCH III: Updates and Verification, *Journal of Physical Oceanography.* 49, 489–517, https://doi.org/10.1175/JPO-D- 18-0137.1

Nose, T., Waseda, T., Kodaira, T., & Inoue, J. (2020). Satellite-retrieved sea ice concentration uncertainty and its effect on modelling wave evolution in marginal ice zones, *Cryosphere*. 14, 2029–2052. https://doiorg/10.5194/tc-14-2029-2020

Rascle, N. & Ardhuin, F. (2013). A global wave parameter database for geophysical applications. Part 2: Model validation with improved source term parameterization, *Ocean Modeling.* 70, 174–188, https://doi.org/10.1016/j.ocemod.2012.12.001

Reynolds, R.W., Smith, T.M., Liu, C., Chelton, D.B., Casey, K.S. & Schlax, M.G. (2007). Daily high-resolution-blended analyses for sea surface temperature. *Journal of Climate*. 20(22),5473–5496.

Rogers, W. E., Babanin, A.V., & Wang, D.W. (2012). Observation consistent input and whitecapping dissipation in a model for wind-generated surface waves: description and simple calculations, *Journal of Atmospheric and Oceanic Technology*. 29, 1329–1346, https://doi.org/10.1175/JTECH-D-11- 00092.1

Saha, S., Moorthi, S., Pan, H.L., Wu, X., Wang, J., Nadiga, S., Tripp, P., Kistler, R., Woollen, J., Behringer, D. & Liu, H. (2010). The NCEP climate forecast system reanalysis. *Bulletin of the American Meteorological Society*. 91(8),1015–1058.

Squire, V.A. (2020). Ocean wave interactions with sea ice: a reappraisal. *Annual Review of Fluid Mechanics*. 52, 37–60.

Taylor, K. E. (2001). Summarizing multiple aspects of model performance in a single diagram. *Journal of Geophysical Research*. 106, 7183–7192, https://doi.org/10.1029/2000JD900719

WAVEWATCH III ® Development Group (WW3DG) (2019). User manual and system documentation of W A VEW A TCH III ® version 6.07, *Technical Note 333*, NOAA/NWS/NCEP/MMAB, College Park, MD, USA, 465 pp.

Zieger, S., Babanin, A. V., Rogers, W. E., & Young, I. R. (2015). Observation-based source terms in the third-generation wave model WAVEWATCH. *Ocean Modelling*, 96, 2–25.

https://doi.org/10.1016/j.ocemod.2015.07.014

References from the Supporting Information

Collins, C. O., III., & Rogers, W. E. (2017). A source term for wave attenuation by sea ice in WAVEWATCH III®, (Technical Memo. NRL/MR7320–17-9726) Naval Research Laboratory.

Doble, M. J., Carolis, G. Ge., Meylan, M. H., Bidlot, J.-R., & Wadhams, P. (2015). Relating wave attenuation to pancake ice thickness, using field measurements and model results, *Geophysical Research Letters,* 42, 4473–4481, doi:10.1002/2015GL063628

Fox, C., & Squire, V. A. (1994). On the obliqure reflexion and transmission of ocean waves at shore fast sea ice. *Philosophical Transactions of the Royal Society of London Series A*, 347, 185–218. https://doi.org/10.1098/rsta.1994.0044

Horvat, C., & Tziperman, E. (2015). A prognostic model of sea-ice floe size and thickness distribution. *Cryosphere*, 9, 2119–4134.

Keller, J. B., (1998). Gravity waves on ice-covered water. *Journal of Geophysical Research,* 103, 7663–7669.

Kohout, A. L., & Meylan, M. H. (2008). An elastic plate model for wave attenuation and ice floe breaking in the marginal ice zone. *Journal of Geophysical Research*, 113, (C9), doi:10.1029/2007JC004434

Kohout, A. L., Williams, M. J. M., Dean, S. M., & Meylan, M. H. (2014). Storm-induced sea-ice breakup and the implications for ice extent. *Nature*, 509, 604–607, doi:10.1038/nature13262

Kohout, A. L., Penrose, B., Penrose, S., & Williams, M.J.M. (2015). A device for measuring wave-induced motion of ice floes in the Antarctic marginal ice zone. *Annals of Glaciology*, 56 (69), 415–424.

Liu, A. K., Holt, B., & Vachon, P. W. (1991). Wave propagation in the marginal ice zone: modelpredictions and comparisons with buoy and synthetic aperture radar data. *Journal of Geophysical Research*, 96, 4605–4621. https://doi.org/10.1029/90JC02267

Liu, A. K., & Mello-Christensen, E. (1988). Wave propagation in a solid ice pack. *Journal of Physical Oceanography*, 18, 1702–1712.

Melyan, M., Bennetts, L. G., & Kohout, A. L. (2014). In situ measurements and analysis of ocean waves in the Antarctic marginal ice zone. *Geophysical Research Letters,* 41, 5046–5051, https://doi.org/10.1002/2014GL060809

Mosig, J. E. M., Montiel, F., & Squire, V. A. (2015). Comparison of viscoelastic-type models for ocean wave attenuation in ice-covered seas. *Journal of Geophysical Research,* 120, 6072–6090. https://doi.org/10.1002/2015JC010881

Rogers, W. E., & Orzech, M. D. (2013). Implementation and testing of ice and mud source functions in WAVEWATCH III®, (Technical Memo. NRL/MR7320–09-9193) Naval Research Laboratory.

Rogers, W. E., Meylan, M. H., & Kohout, A. L. (2018). Frequency distribution of dissipation of energy of ocean waves by sea ice using data from Wave Array 3 of the ONR "Sea State" field experiment, (Technical Memo. NRL/MR7322–18-9801) Naval Research Laboratory.

Rogers, W. E., Meylan, M. H., & Kohout, A. L. (2021). Estimates of spectral wave attenuation in Antarctic sea ice using mode/data inversion. *Cold Regions Science and Technology,* 182, https://doi.org/10.1016/j.coldregions.2020.103198

Thomson, J. (2012). Wave breaking dissipation observed with SWIFT drifters. *Journal of Atmospheric and Oceanic Technology,* 29, 1866–1882, doi:10.1175/JTECH-D-12-00018.1

Tolman, H. L. (2003). Treatment of unresolved islands and ice in wind wave models. *Ocean*

Modelling, 5(3), 219–231. https://doi.org/10.1016/S1463-5003(02)00040-9

Wadhams, P. & J. Thomson. (2015). The Arctic Ocean cruise of R/V Sikuliaq 2015, An investigation of waves and the advancing ice edge. *II Polo*, 70(4), 9–38.

Wadhams, P., V. A. Squire, D. J. Goodman, A. M. Cowan, & S. C. Moore (1988). The attenuation rates of ocean waves in the marginal ice zone, *Journal of Geophysical Research,* 93, 6799–6818.

Wang, R., & H. H. Shen (2010). Gravity waves propagation into an ice-covered ocean: A viscoelastic model. *Journal of Geophysical Research,* 115, C06024, https://doi.org/10.1029/2009JC005591